JOURNAL OF SPACECRAFT AND ROCKETS
Vol. 33, No. 6, November–December 1996

Formulation and Analysis of Launch Vehicle Maneuvering Loads

K. W. Dotson*
The Aerospace Corporation, Los Angeles, California 90009-2957
and
S. B. Tiwari†
Lockheed Martin Corporation, Denver, Colorado 80201-0179

A formulation for launch vehicle loads induced by maneuvering through winds is presented. The distinction between these dynamic loads and the static aeroelastic loads computed on the day of launch is explained. An analysis of maneuvering loads is presented for an actual mission of the Titan IV launch vehicle. The inputs from the trajectory simulation, the magnitudes of the maneuvering loads, and the effects of aerodynamic stiffness and damping are assessed for this mission. Titan IV experience indicates that this loads event is the primary contributor to the system response below approximately 5 Hz and that loads for this class of expendable launch vehicles may be significantly underpredicted if maneuvering is neglected.

Nomenclature

C = aerodynamic force coefficient, dimensionless
$\bar{C}$ = coefficient for static aeroelastic bending moment at a given Mach number, lbf-in. (N-m)
$[C']$ = system diagonal matrix of partial derivatives of C with respect to angle of attack, rad^{-1}
$[C^*]$ = system modal damping matrix, lbf-s/in. (N-s/m) and lbf-s/rad (N-s/rad)
$\{f(t)\}$ = vector of system external forces, lbf (N)
$[I]$ = system modal mass matrix (identity matrix), lbm (kg)
$\{I\}$ = identity vector, dimensionless
$[K]^{-1}$ = system elastic flexibility matrix, in./lbf (m/N) and rad/lbf (rad/N)
$[LTMD]$ = transformation matrix for displacement-based loads; e.g., lbf/in. (N/m) and lbf-in./in. (N-m/m)
$[LTMF]$ = transformation matrix for pseudostatic loads, lbf/lbf (N/N) and lbf-in./lbf (N-m/N)
$[LTMQ]$ = transformation matrix for maneuvering loads, lbm (kg) and lbm-in. (kg-m)
$\{l(t)\}$ = vector of loads induced by the aerodynamic and control forces, lbf (N) and lbf-in. (N-m)
$[M]$ = physical system mass matrix, lbm (kg)
$M(t)$ = bending moment time history, lbf-in. (N-m)
$\bar{M}$ = mean bending moment, lbf-in. (N-m)
$\tilde{M}$ = dispersed bending moment, lbf-in. (N-m)
$\hat{M}$ = bending moment that maximizes the total moment, lbf-in. (N-m)
$[N]$ = system aerodynamic stiffness matrix, lbf/rad (N/rad)
$[\dot{N}]$ = system aerodynamic damping matrix, lbf-s/in. (N-s/m)
Q = dynamic pressure at the flight time being analyzed, lbf /in.^{2} (N/m^2)
$\{q(t)\}$ = vector of system generalized translations and rotations, in. (m) and rad
$\{\dot{q}(t)\}$ = vector of system generalized translational and rotational velocities, in./s (m/s) and rad/s
$\{\ddot{q}(t)\}$ = vector of system generalized translational and rotational accelerations, in./s^2 (m/s^2) and rad/s^2
S = reference area, in.^{2} (m^2)
t = time after solid rocket motor ignition, s
V = relative wind velocity, in./s (m/s)
$\{x(t)\}$ = vector of physical system translations and rotations, in. (m) and rad
$\dot{y}(t)$ = velocity in the direction of the y axis, in./s (m/s)
$\dot{z}(t)$ = velocity in the direction of the z axis, in./s (m/s)
$\alpha(t)$ = rigid-body angle of attack in the pitch plane, rad or deg
$\beta(t)$ = rigid-body angle of attack in the yaw plane (also called side slip), rad or deg
$\{\Gamma\}$ = aerodynamic force vector, lbf/rad (N/rad)
$\theta(t)$ = rotation, rad
$[\phi]$ = system modes matrix, dimensionless
$[\omega^2]$ = system modal stiffness matrix, lbf/in. (N/m) and lbf/rad (N/rad)

Subscripts

a = autopilot noise
b = buffet
c = control; also, physical control force application points
d = dispersions on thrust, dynamic pressure, autopilot gains, etc.
e = elastic motion
ee = elastic motion neglecting rigid-body contribution
er = elastic motion induced by rigid-body motion
f = physical force application points
g = gust
j = node number
m = maneuvering
nom = nominal value
p = pitch plane
ps = pseudostatic
r = rigid-body motion
$\hat{r}$ = rotational motion
re = rigid-body motion induced by elastic motion
rr = rigid-body motion neglecting elastic contribution
stel = static aeroelastic
T = total
t = translational motion
y = direction of, or rotation about, the y axis; also, the yaw plane
z = direction of, or rotation about, the z axis

Received Feb. 28, 1996; revision received July 5, 1996; accepted for publication July 30, 1996.

*Engineering Specialist, Vehicle Systems Division, Structural Dynamics Department, P.O. Box 92957-M4/911. Member AIAA.
†Staff Engineer, Space Launch Systems, Loads and Dynamics Department, P.O. Box 179-L5505. Member AIAA.

Introduction

ALONG with the liftoff event, maximum airloading induces the most important loads for the design of an expendable launch vehicle.[1] In contrast, for reusable systems such as the Space Shuttle, loads induced by landing can be critical.[2] The maximum airloads are analyzed as a combination of static and dynamic effects. Since a large part of the maximum airloads are attributable to the wind profile, the static aeroelastic (STEL) loads may be treated deterministically and computed on the day of launch based on wind soundings taken as close as possible to the actual launch time.[1] The dynamic components of the maximum airloads in this approach are computed long before the launch date, are treated statistically, and are combined on the day of launch with the STEL loads based on the measured wind. Mean and dispersed values for each of the dynamic load components are estimated, and then total loads are computed using a loads combination equation such that 1) the dispersed portions of the dynamic loads components are root-sum-squared, 2) the mean values of the dynamic components are added to the root-sum-squared dispersed loads, and 3) the total load is defined as the sum of this result and the STEL load computed on the day of launch.[3] The loads combination equation and conservatism of the analysis predictions are briefly discussed in Appendix A.

A schematic indicating the maximum airloads analysis procedure used for the Titan IV is shown in Fig. 1. The highlighted boxes indicate the components of this process that concern the analysis of maneuvering loads and their use in the computation of total system loads. For the Titan IV, the dynamic components of the maximum airloads consist of those induced by buffeting, gust, the feedback control system, and maneuvering. Loads dispersions that account for tolerances on the thrust, dynamic pressure, autopilot gains, etc., are also included in the loads combination on the day of launch but, for brevity, are not illustrated in Fig. 1.

Buffet loads account for fluctuating pressures caused by unsteady aerodynamics and flow separation during transonic flight. Loads induced by the feedback control system include the effects of noise in the autopilot and limit cycling caused by control nonlinearities. Gust loads account for the relatively small-scale variations in the wind, i.e., short duration wind turbulence, that are not included in the wind sounding; these features are not included because of the relatively short rise rate of the balloons used for the wind soundings.

Many vehicles (including Titan, Delta, and Atlas) use prelaunch wind sounding just prior to flight to define the vehicle's steering program, which minimizes the angle of attack relative to the measured wind. Loads are reduced during flight by the programmed steering and by the onboard control system, which measures accelerations and steers the vehicle into the sensed wind. Maneuvering loads account for the dynamic elastic response of the vehicle to the steering commands during its flight through the wind profile.[1] This response is induced by fluctuations in the wind soundings and by the control system's response to them. Maneuvering of the Titan IV system is a major contributor to the vehicle's low frequency loads. System responses below approximately 5 Hz are generally underestimated if the effects of vehicle maneuvering are neglected. For the Titan IV this frequency range includes the first three bending modes in both the yaw and pitch planes.

The existing literature on maximum airloading does not address the formulation of maneuvering loads. The objective of this paper is to describe a methodology for the computation of these loads including a detailed definition of the mathematical implementation. The forcing functions defined by the trajectory simulation, the relationship of maneuvering loads with the static aeroelastic loads computed on the day of launch, and the effects of aerodynamic stiffness and damping are also investigated.

Formulation of Maneuvering Loads

System Equations of Motion

The modal equations of motion for the system subjected to the maneuvering forcing functions are defined by

$$[I]\{\ddot{q}(t)\} + [C^*]\{\dot{q}(t)\} + [\omega^2]\{q(t)\} = [\phi]_f^T\{f(t)\} \qquad (1)$$

The vector $\{f(t)\}$ is composed of the aerodynamic forces and the control forces, which steer the vehicle into the wind. For the Titan IV, the modal matrices are generated using the subsystem dynamic models and the Benfield–Hruda component coupling procedure.[4] Equation (1) is solved for the time histories $\{\ddot{q}(t)\}$, $\{\dot{q}(t)\}$, and $\{q(t)\}$.

The system mass over the duration of the analysis, 5 s, is not constant because the solid rocket motor (SRM) propellant is being consumed. The equations of motion, however, are assumed to be stationary, and the system mass matrix corresponds to the midpoint of the analysis time duration. Parametric studies conducted during the course of this work proved that this assumption is acceptable for airloads analyses less than 10 s in duration.

Forcing Functions

The Titan IV launch vehicle and its coordinate system are shown in Fig. 2. A three-dimensional maneuvering loads analysis is conducted. The aerodynamic coefficients for the yaw and pitch planes are assumed to be uncoupled. The latter assumption has been shown to be acceptable for the Titan IV.[5] The yaw and pitch aerodynamic forces are lumped at 52 stations along the launch vehicle. The control forces are applied at the gimbal points of the SRMs. For the Titan IV, a set of 10 wind cases are randomly selected from the

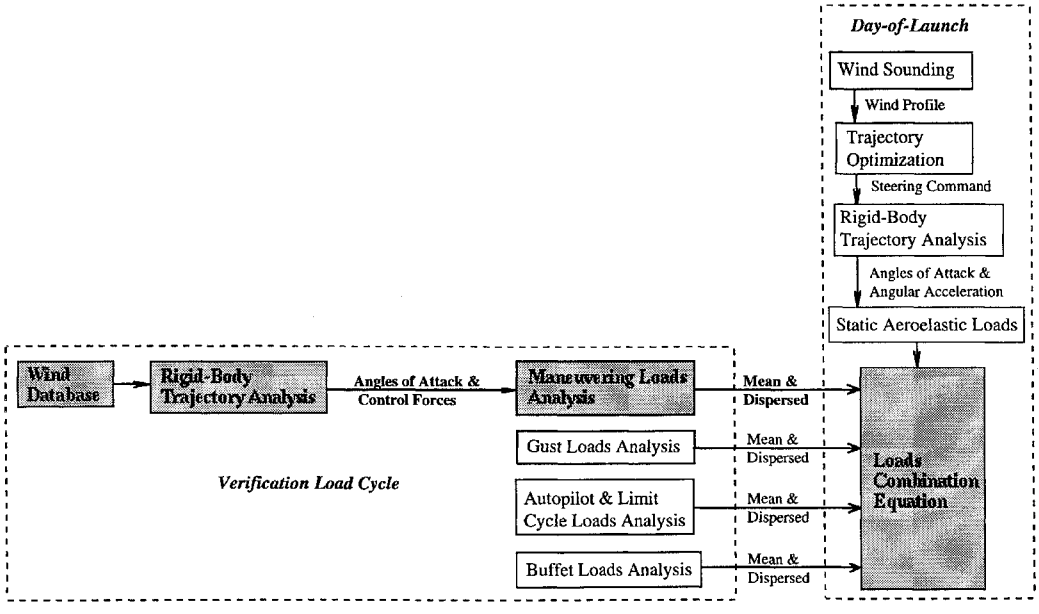

Fig. 1 Titan IV maximum airloads analysis procedure.

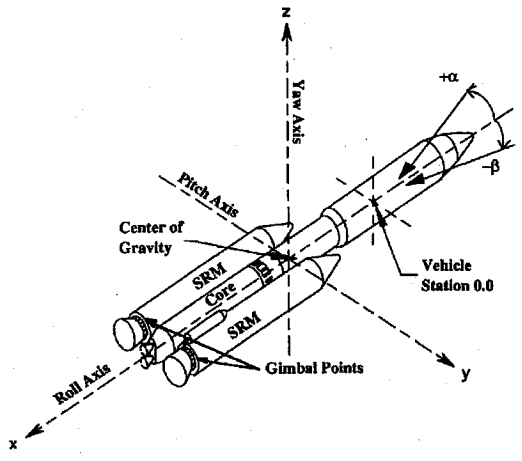

Fig. 2 Titan IV coordinate system for launch vehicle stations and aerodynamic loading.

wind database to statistically define the mean and dispersed values of the maneuvering loads. The wind database is composed of 99 wind cases derived from Jimsphere wind soundings corresponding to the time of launch.

The forcing functions for each of the 10 wind cases in the maneuvering loads analysis are obtained by simulating the trajectory for the mission considered (see Fig. 1). For a given wind case, the control forces correspond to the steering commands during the vehicle's simulated flight through the wind profile. The control forces, therefore, stabilize the launch vehicle while steering it in the programmed trajectory. The vehicle elastic motion induced by this steering generates the maneuvering loads. As stated earlier, for the Titan IV system these loads must be accounted for in the vehicle structural analysis and design.

The results of the maneuvering loads analysis are obviously dependent on the accuracy of the trajectory simulation. The objective of the simulation is to validate that the spacecraft will be placed in the targeted orbit given the performance characteristics of the launch vehicle and the environments it is expected to experience during flight. Elastic motion is of secondary importance for this validation and the Titan IV simulation currently assumes that the launch vehicle acts as a rigid body during flight. This assumption is common in the industry. Because the vehicle is considered to act as a rigid body, changes in the angle of attack caused by local rotation and lateral velocity are not accounted for in the trajectory simulation. These effects, called aeroelastic stiffness and damping, respectively, modify the system equations of motion as shown in Appendix B. Recent studies using quasistatic[6] and simplified dynamic[7] trajectory simulations, which include elastic deformation of the launch vehicle, have confirmed that the angles of attack and control forces are somewhat different from those for a rigid-body trajectory simulation, especially for time points close to the maximum dynamic pressure.

Note that, although elastic motion is neglected in the trajectory simulation, the aerodynamic and control forces that it defines generate elastic loads when the launch vehicle equations of motion [Eq. (1)] include the elastic system modes, as does the maneuvering loads analysis. The elastic motion and corresponding maneuvering loads would, of course, be more accurately predicted if the trajectory simulation included the elastic body effects. This enhancement is being considered for the Titan IV. Uncertainties in the predicted maneuvering loads introduced by the trajectory simulation's rigid-body assumption are discussed in more detail in a subsequent section.

Time histories of the summations of the aerodynamic and control forces are provided in Fig. 3 to illustrate their signatures and magnitudes. The results in the yaw and pitch planes are shown for an example wind case applied to a Titan IV mission. The time period illustrated is centered about the predicted Mach 1.0 time point, 42 s, for this particular mission. Note that, as required for vehicle stability, the control force time history has the same general trend and roughly the same amplitude as the aerodynamic force resultant. The former, however, lags in time behind the latter because the autopilot, which controls these forces, does not react instantaneously.

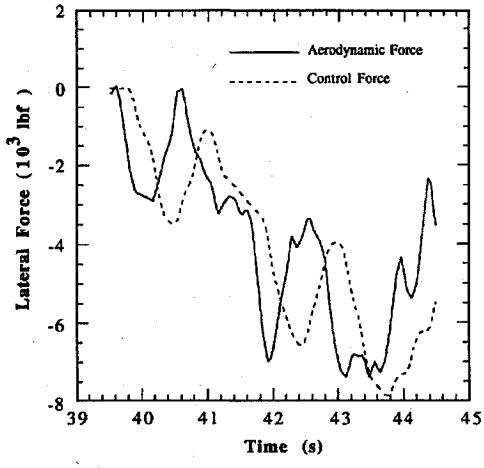

a) Yaw plane

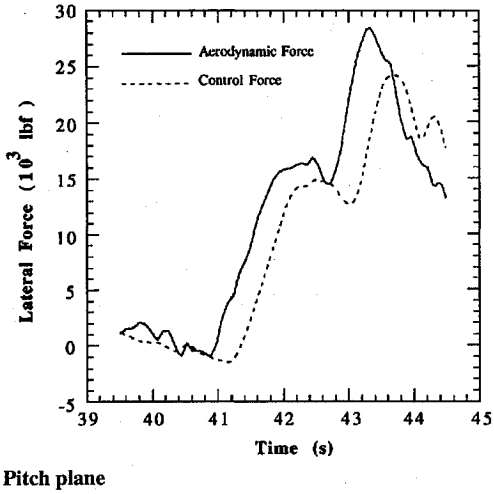

b) Pitch plane

Fig. 3 Aerodynamic and control forces from the Titan IV trajectory simulation for the example wind case.

Rigid-Body Responses

The magnitudes of the input angles of attack for the example wind case and the resulting rigid-body angular accelerations, recovered using Eq. (1), are shown in Fig. 4. The numbers in parentheses in the figure legends refer, throughout this paper, to the equations from which the results were obtained. Figure 4 provides a check that the open-loop responses defined by Eq. (1) are consistent with those for the rigid-body trajectory simulation, which produced the angles of attack and control forces. The rigid-body angular acceleration time histories vary about zero, indicating that, as expected, the launch vehicle does not tumble but remains stable during its response to the wind. The vehicle, however, is not balanced at every instant of time because the aerodynamic and control forces are slightly out of phase. In the balanced STEL loads analysis conducted for the Titan IV it is assumed that the dashed curves in Fig. 4 always equal zero. The impact of this assumption on static aeroelastic loads is investigated later in this paper.

Loads Transformations

The derivation of the loads transformation equation begins with the following expression for the launch vehicle loads induced by the inputs from the trajectory simulation,

$$\{l(t)\} = [LTMD]\{x(t)\} = [LTMD][\phi]\{q(t)\} \qquad (2)$$

The matrix $[LTMD]$ is produced from the finite element model for the launch vehicle and generally corresponds to the six loads (three forces and three moments) at each of the vehicle nodes. For example, the (1, 2) element of this matrix is defined as the force (or moment) corresponding to the first element of $\{l(t)\}$ induced when the displacement (or rotation) corresponding to the second element of $\{x(t)\}$ has a unit value and all of the remaining displacements (and rotations) of $\{x(t)\}$ equal zero.

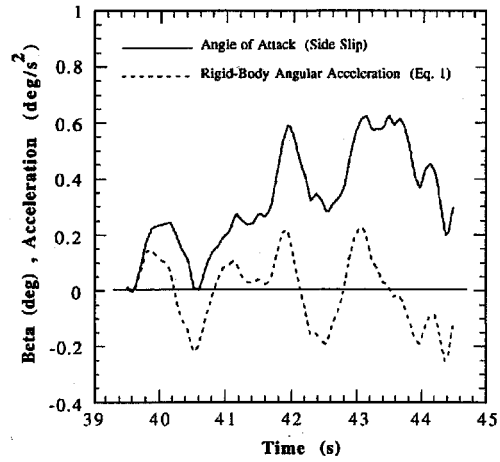

a) Yaw plane

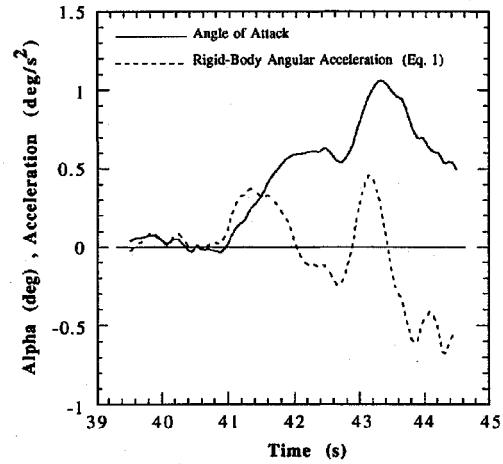

b) Pitch plane

Fig. 4 Angle-of-attack and rigid-body angular acceleration time histories for the example wind case.

The use of generalized displacements is inefficient in the sense that a large number of modes must be retained for loads convergence. The mode-acceleration method[8] is traditionally used instead because more modes can be truncated during component mode synthesis without adverse effects on loads convergence. In this method the loads are expressed as

$$\{l(t)\} = [LTMD][K]^{-1}(\{f(t)\} - [M][\phi_e]\{\ddot{q}_e(t)\}) \tag{3}$$

in which

$$[K]^{-1} = [\phi_e]\left[\omega_{ee}^2\right]^{-1}[\phi_e]^T \tag{4}$$

For the maneuvering loads analysis, the mode-acceleration method has the added advantage that it defines the pseudostatic (PS) and dynamic components of the loads induced by the applied aerodynamic and control forces. The former are analogous to the balanced STEL loads computed on the day of launch and must be deleted so that they are not accounted for twice in the loads combination equation (see Fig. 1). The loads induced by rigid-body accelerations, similarly, are omitted in Eq. (3) because they are analogous to rigid-body loads computed on the day of launch. Maneuvering loads are consequently defined simply by the load component corresponding to the dynamic elastic motion. The day-of-launch loads, of course, do not exactly equal their counterparts in the maneuvering loads analysis because they correspond to the measured wind sounding, not to any of the maneuvering analysis wind cases.

Equation (4) is next substituted into Eq. (3) and the system modes from the component mode synthesis are forced to be orthonormal with respect to the system mass matrix.[9] The orthogonality constraint improves the accuracy of the loads transformation by eliminating inaccuracies in the triple product introduced by modal truncation and yields loads that are essentially identical to those obtained by grounding the free-free system; the negligible differences between these two approaches are attributable to the omission of damping in Eq. (3). The resulting launch vehicle loads formulation is given by

$$\{l(t)\} = [[LTMF] \quad [LTMQ]] \begin{Bmatrix} \{f(t)\} \\ \{\ddot{q}_e(t)\} \end{Bmatrix} \tag{5}$$

in which

$$[LTMF] = [LTMD][\phi_e]\left[\omega_{ee}^2\right]^{-1}[\phi_e]^T \tag{6}$$

and

$$[LTMQ] = -[LTMD][\phi_e]\left[\omega_{ee}^2\right]^{-1} \tag{7}$$

Finally, the pseudostatic and maneuvering loads are defined by

$$\{l_{ps}(t)\} = [LTMF]\{f(t)\} \tag{8}$$

$$\{l_m(t)\} = [LTMQ]\{\ddot{q}_e(t)\} \tag{9}$$

Static Aeroelastic Loads

The pseudostatic loads in Eq. (8) are assessed in this section to provide a reference for the magnitudes of the maneuvering loads. The conservatism introduced by the assumption of a balanced condition in the static aeroelastic loads analysis and the effects of aerodynamic stiffness on static aeroelastic loads are also quantified.

Loads Transformation Including Local Rotation

The effects of local rotation, called aerodynamic stiffness, are included in the balanced STEL loads analysis, even though the rigid-body trajectory simulation that generates the angles of attack used for the STEL loads analysis, by definition, does not. The impact of aerodynamic stiffness on static aeroelastic loads is investigated in this subsection to establish if its effect is secondary, as it is for trajectory design.

It is easily shown that the recovery of pseudostatic loads with aerodynamic stiffness is identical to that described in Eqs. (6) and (8) except that the elastic flexibility matrix is redefined as

$$[K]^{-1} = [\phi_e]\left(\left[\omega_{ee}^2\right] + [N_{ee}]\right)^{-1}[\phi_e]^T \tag{10}$$

The system aerodynamic stiffness and damping matrices are derived in Appendix B. The pseudostatic loads transformation with aerodynamic stiffness is given by

$$[LTMF] = [LTMD][\phi_e]\left(\left[\omega_{ee}^2\right] + [N_{ee}]\right)^{-1}[\phi_e]^T \tag{11}$$

which is equivalent to the formulation for the STEL loads prior to enforcing the constraint that the launch vehicle remain balanced at every instant of time.

Balanced Static Aeroelastic Loads

If it is assumed that the control and aerodynamic forces are balanced at every instant of time, the control forces can be eliminated as an independent variable. The control and aerodynamic loads in a particular plane then are proportional to the angle of attack in that plane. Similarly, the system loads induced by the aerodynamic and control forces are strictly functions of the angles of attack. Time histories for the balanced STEL yaw and pitch moments are expressed as

$$M_y(t) = \bar{C}_{y,\text{nom}} \frac{Q}{(Q\beta)_{\text{nom}}} \beta(t) \tag{12}$$

$$M_p(t) = \bar{C}_{p,\text{nom}} \frac{Q}{(Q\alpha)_{\text{nom}}} \alpha(t) \tag{13}$$

Similar expressions exist for yaw and pitch shear loads but, for brevity, comparisons of analytical results will be restricted to launch vehicle bending moments. The conclusions for the bending moments apply to the shear loads as well. Similarly, conclusions herein based on mean loads also generally apply to the corresponding dispersed loads.

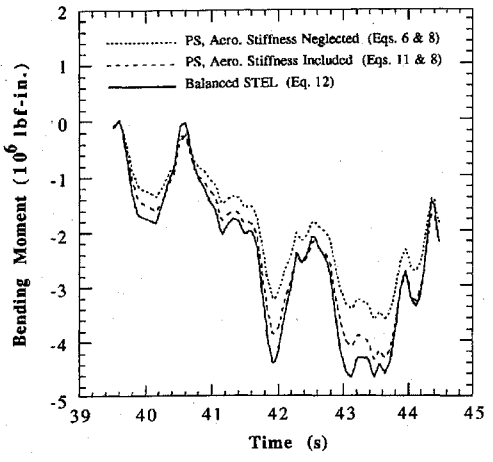

a) Yaw plane

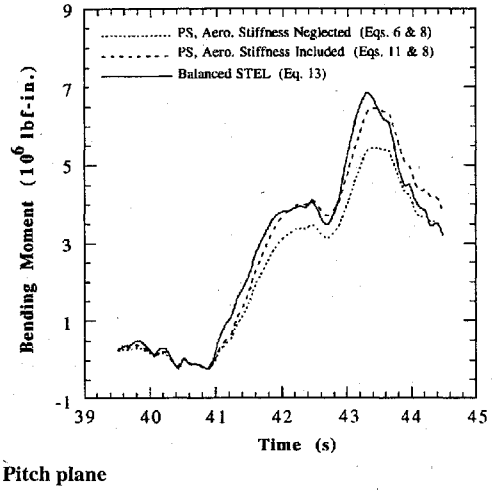

b) Pitch plane

Fig. 5 Static component of bending moments at vehicle station 374 for the example wind case.

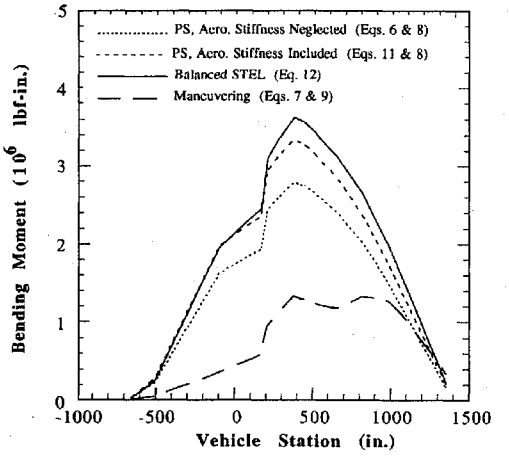

a) Yaw plane

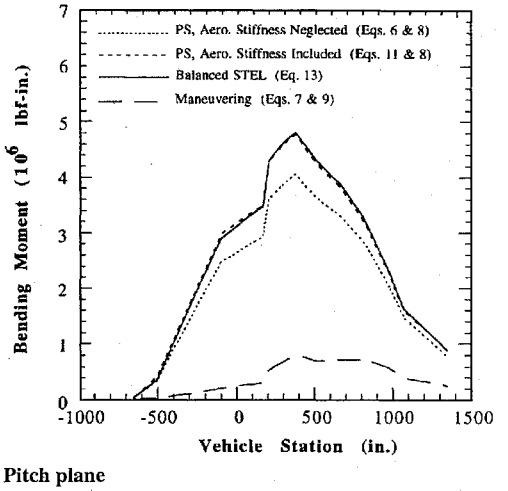

b) Pitch plane

Fig. 6 Mean static and maneuvering bending moments (based on set of 10 wind cases) for vehicle stations monitored on the day of launch.

Comparisons for a Titan IV Mission

Time histories of the yaw and pitch bending moment at vehicle station 374 are shown in Fig. 5 for a Titan IV mission subjected to the example wind case. Vehicle station 374 is on the core approximately one-fourth of the distance between the vehicle's origin and the end of the SRM nozzles (see Fig. 2). This location was chosen to illustrate the results because the bending moments are a maximum at this point. For the Titan IV coordinate system, positive values of β and α produce, respectively, negative yaw plane and positive pitch plane bending moments. When this sign difference for the yaw plane is taken into consideration, it is evident that the bending moment time histories in Fig. 5 have the same character as the angle-of-attack time histories in Fig. 4.

Figure 5 also shows that the inclusion of aerodynamic stiffness increases the absolute maximum value of the pseudostatic moments by approximately 20% and that the pseudostatic (with aerodynamic stiffness) and balanced STEL time histories are in reasonable agreement. The absolute maximum values of the pseudostatic time histories, however, are lower than those for the balanced STEL time histories because the lag in time between the control and aerodynamic forces generally provides some relief for the elastic loads. For the example wind case, a 6% reduction in the absolute maximum values of the yaw and pitch static aeroelastic bending moments (and a corresponding increase in launch availability) could be achieved by modifying the STEL methodology to account for the lag time between the aerodynamic and control forces.

Mean values of the static aeroelastic and maneuvering moments for the vehicle stations monitored on the day of launch are compared in Fig. 6. For a given moment, mean value is defined herein as the average of the absolute maxima from the time histories for the 10 wind cases. The mean maneuvering moments for the yaw and pitch planes at vehicle station 374 are 37 and 16% of the mean balanced STEL moments, respectively. Loads induced by the dynamic elastic motion of the Titan IV as it maneuvers through winds, therefore, are a significant contributor to the total loads experienced during the period of maximum airloading and cannot be ignored. This may well be the case for other launch vehicles in this class.

Figure 6 also illustrates that, for the wind set considered, the loads relief due to the control force lag time is, on average, greater in the yaw plane than in the pitch plane. The salient parameter for the loads reduction is the ratio of the lag time and the major period of the wind force. The smaller this ratio, the smaller the loads relief. The average lag times in the yaw and pitch planes for the wind set are 0.5 and 0.3 s, respectively, and the average periods of the wind forces are 1.4 and 1.8 s.

Effects of Aerodynamic Stiffness and Damping on Maneuvering Loads

In this section the effect on maneuvering loads of the omission of aerodynamic stiffness and damping from the trajectory simulation is estimated. The modal equations of motion including aerodynamic stiffness and damping are given by

$$[I]\{\ddot{q}(t)\} + ([C^*] + [\dot{N}])\{\dot{q}(t)\} + ([\omega^2] + [N])\{q(t)\} = [\phi]_f^T\{f(t)\} \tag{14}$$

Figure 7 shows time histories of the vehicle rigid-body angular accelerations that result from these equations of motion with forcing functions defined by the rigid-body trajectory simulation. A set of three results are provided for the example wind case to illustrate the effects of the rigid-body and elastic components of the aerodynamic stiffness and damping matrices on the rigid-body response. Referring to Eq. (B15), the results correspond to full inclusion of the

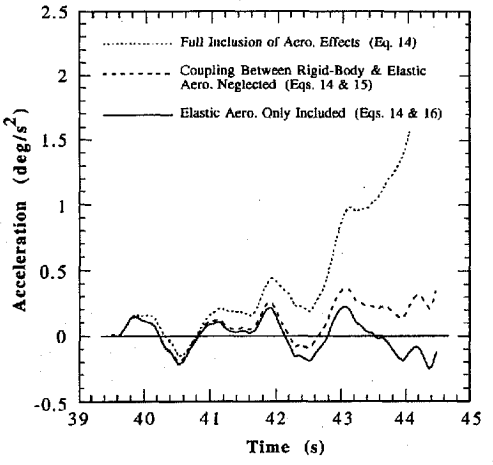

a) Yaw plane

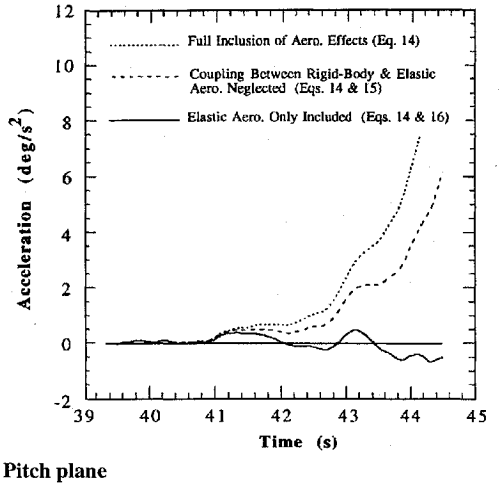

b) Pitch plane

Fig. 7 Effects of aerodynamic stiffness and damping on rigid-body angular acceleration time histories for the example wind case.

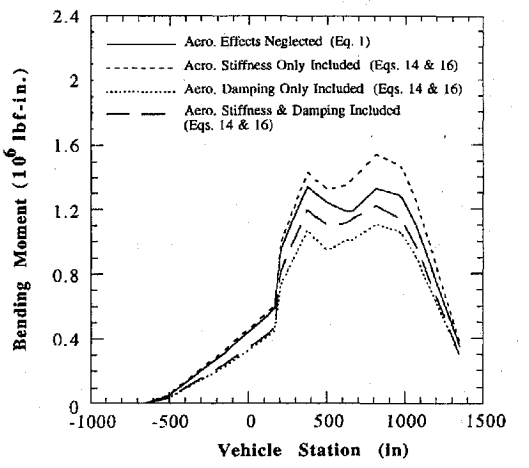

a) Yaw plane

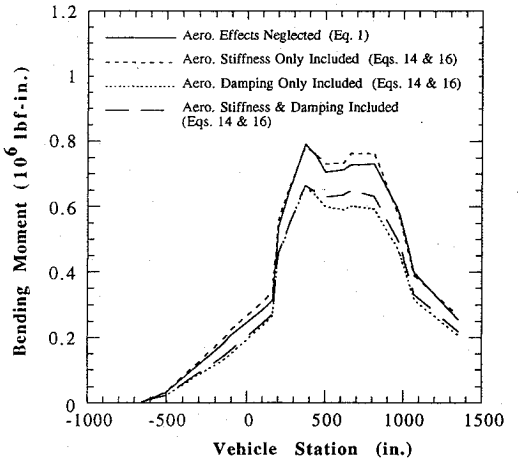

b) Pitch plane

Fig. 8 Effects of elastic aerodynamic stiffness and damping on mean maneuvering bending moments (based on set of 10 wind cases) for vehicle stations monitored on the day of launch.

aerodynamic effects; inclusion of the aerodynamic effects but with coupling between the rigid body and elastic modes eliminated, i.e.,

$$[N_{re}] = [N_{er}] = 0; \qquad [\dot{N}_{re}] = [\dot{N}_{er}] = 0 \tag{15}$$

and inclusion of the aerodynamic effects only for the elastic modes, i.e.,

$$[N_{rr}] = [N_{re}] = [N_{er}] = 0; \qquad [\dot{N}_{rr}] = [\dot{N}_{re}] = [\dot{N}_{er}] = 0 \tag{16}$$

The latter also corresponds to the complete omission of aerodynamic stiffness and damping from the rigid-body equations of motion and yields responses that are identical to those predicted by the trajectory simulation.

Because an open-loop transient analysis is conducted, the predicted response of the launch vehicle will not remain stable if aerodynamic stiffness and damping significantly affect the forcing functions. For the example shown in Fig. 7, the forcing functions are only adequate for analyses with aerodynamic stiffness and damping that are not longer than about 2 s in duration. Inclusion of the real phenomena of aeroelastic stiffness and damping in the trajectory simulation, therefore, would be expected to have an impact on the overall trend of the forcing functions used for maneuvering loads analyses. This conclusion is consistent with the findings of Ref. 7.

Figure 7 confirms that the launch vehicle remains stable when aerodynamic stiffness and damping corresponding to only the elastic modes are retained in the equations of motion. The mean maneuvering bending moments derived from the equations of motion for this case [Eqs. (14) and (16)] are compared in Fig. 8 with the current maneuvering moments derived from equations of motion that neglect the aerodynamic effects [Eq. (1)]. All of the results presented in Fig. 8 were computed using Eqs. (7) and (9) with the elastic generalized accelerations from the appropriate equations of motion. Aerodynamic stiffness and damping are examined separately and together. As expected, aerodynamic stiffness and damping increase and decrease, respectively, maneuvering loads relative to those without these effects. For the Titan IV mission and wind set analyzed, the net result is a reduction (of up to 24%) in the mean maneuvering bending moments. The current maneuvering loads, which neglect the effects of aerodynamic stiffness and damping, are therefore conservative. More accurate maneuvering loads predictions could be achieved by modifying the trajectory simulation to include elastic motion, even though these effects are of secondary importance for trajectory design.

Conclusions

For the Titan IV, maneuvering loads are a significant contributor to the total loads experienced during the period of maximum airloading. The Titan IV loads methodology in which the static aeroelastic and dynamic components are separated is conservative. This approach allows the computation of the static aeroelastic loads during day-of-launch activity using measured winds. The assumption of a balanced condition for the computation of static aeroelastic loads is conservative. A reduction in the predicted static aeroelastic loads, and a corresponding increase in launch availability, could be achieved by modifying the STEL methodology to account for the lag time between the aerodynamic and control forces. The maneuvering forcing functions currently defined by a rigid-body trajectory simulation produce conservative loads. Enhancements to the trajectory simulation to include elastic deformation would result in more accurate loads predictions.

Appendix A: Combination of Airload Components

The combination of the airload components for launch vehicle bending moments is summarized in this Appendix. Reference 3 contains a more thorough description of the airloads combination equation. The gust, buffet, autopilot noise/limit cycle, maneuvering, and STEL loads results and the dispersions due to tolerances on thrust, dynamic pressure, autopilot gains, etc., are combined to produce the maximum total moment at a given vehicle station as follows.

The mean and dispersed bending moments in the yaw and pitch planes are given by

$$\bar{M}_y = \bar{M}_{g,y} + \bar{M}_{b,y} + \bar{M}_{m,y} + \bar{M}_{a,y} \tag{A1}$$

$$\bar{M}_p = \bar{M}_{g,p} + \bar{M}_{b,p} + \bar{M}_{m,p} + \bar{M}_{a,p} \tag{A2}$$

$$\tilde{M}_y = \left(\tilde{M}_{g,y}^2 + \tilde{M}_{b,y}^2 + \tilde{M}_{m,y}^2 + \tilde{M}_{a,y}^2 + \tilde{M}_{d,y}^2\right)^{\frac{1}{2}} \tag{A3}$$

$$\tilde{M}_p = \left(\tilde{M}_{g,p}^2 + \tilde{M}_{b,p}^2 + \tilde{M}_{m,p}^2 + \tilde{M}_{a,p}^2 + \tilde{M}_{d,p}^2\right)^{\frac{1}{2}} \tag{A4}$$

The total moment is given by

$$M_T = \left[(M_{\text{stel},y} + \hat{M}_y)^2 + (M_{\text{stel},p} + \hat{M}_p)^2\right]^{\frac{1}{2}} \tag{A5}$$

where $(\hat{M}_y, \hat{M}_p)$ is the point on an ellipse in the (M_y, M_p) plane that produces the maximum value of M_T. The origin of the ellipse is $(M_{\text{stel},y}, M_{\text{stel},p})$ and its axes are $\bar{M}_y + \tilde{M}_y$ and $\bar{M}_p + \tilde{M}_p$.

The total moment represents the predicted load with 99.73% probability of nonexceedance and 90% confidence level based on a Gaussian distribution. Because 10 wind cases are used in the maneuvering loads analysis, small sample statistics are taken into account and a confidence factor of 4.6, instead of the usual 3.0, is used as a multiplier to the standard deviation in calculating the dispersed maneuvering loads.

The conservatism of the airloads combination has been validated using Titan IV flight data. Buffet predictions alone generally bound flight accelerations in the frequency range 5–40 Hz. A statistical analysis of accelerations from 14 missions also confirmed that the sum of the maneuvering and buffet predictions bound flight data in the frequency range 0–5 Hz. However, when the maneuvering loads event is omitted, flight accelerations are underpredicted in this frequency range.

Appendix B: Derivation of Aerodynamic Stiffness and Damping

The modal equations of motion are defined by

$$[I]\{\ddot{q}(t)\} + [C^*]\{\dot{q}(t)\} + [\omega^2]\{q(t)\} = [\phi]_f^T\{f(t)\} \tag{B1}$$

In the Titan IV coordinate system, at node j of the dynamic model, the aerodynamic forces in the yaw and pitch planes are defined by

$$f_{y,j}(t) = QS\left(\frac{\partial C_y}{\partial \beta}\right)_j \beta_{T,j}(t) \tag{B2}$$

$$f_{z,j}(t) = QS\left(\frac{\partial C_p}{\partial \alpha}\right)_j \alpha_{T,j}(t) \tag{B3}$$

in which the terms in the parentheses represent the change in the dimensionless aerodynamic normal force with angle of attack at the node j. The angles of attack at the node j including the local effects are defined by

$$\beta_{T,j}(t) = \beta(t) + \frac{\dot{y}_j(t)}{V} + \theta_{z,j}(t) \tag{B4}$$

$$\alpha_{T,j}(t) = \alpha(t) - \frac{\dot{z}_j(t)}{V} + \theta_{y,j}(t) \tag{B5}$$

Substituting Eqs. (B4) and (B5) into Eqs. (B2) and (B3), and writing the equations for the dynamic model in matrix notation yield

$$\{f_y(t)\} = QS[C_y'](\{I\}\beta(t) + \{\dot{y}(t)/V\} + \{\theta_z(t)\}) \tag{B6}$$

$$\{f_p(t)\} = QS[C_p'](\{I\}\alpha(t) - \{\dot{z}(t)/V\} + \{\theta_y(t)\}) \tag{B7}$$

Substituting Eqs. (B6) and (B7) into Eq. (B1) yields

$$[I]\{\ddot{q}(t)\} + ([C^*] + [\dot{N}_y] + [\dot{N}_p])\{\dot{q}(t)\} + \left([\omega^2] + [N_y] + [N_p]\right)\{q(t)\} = \{\Gamma_y\}\beta(t) + \{\Gamma_p\}\alpha(t) + [\phi]_c^T\{f_c(t)\} = [\phi]_f^T\{f(t)\} \tag{B8}$$

in which

$$[N_y] = -QS[\phi_{ty}]^T[C_y'][\phi_{\dot{r}z}] \tag{B9}$$

$$[N_p] = -QS[\phi_{tz}]^T[C_p'][\phi_{\dot{r}y}] \tag{B10}$$

$$[\dot{N}_y] = -(QS/V)[\phi_{ty}]^T[C_y'][\phi_{ty}] \tag{B11}$$

$$[\dot{N}_p] = (QS/V)[\phi_{tz}]^T[C_p'][\phi_{tz}] \tag{B12}$$

$$\{\Gamma_y\} = QS[\phi_{ty}]^T[C_y']\{I\} \tag{B13}$$

$$\{\Gamma_p\} = QS[\phi_{tz}]^T[C_p']\{I\} \tag{B14}$$

Expanding Eq. (B8) into submatrices for the rigid-body and elastic modes yields

$$\begin{bmatrix}[I] & [0]\\ [0] & [I]\end{bmatrix}\begin{Bmatrix}\{\ddot{q}_r(t)\}\\ \{\ddot{q}_e(t)\}\end{Bmatrix} + \left(\begin{bmatrix}[0] & [0]\\ [0] & [C_{ee}^*]\end{bmatrix} + \begin{bmatrix}[\dot{N}_{rr}] & [\dot{N}_{re}]\\ [\dot{N}_{er}] & [\dot{N}_{ee}]\end{bmatrix}\right) \times \begin{Bmatrix}\{\dot{q}_r(t)\}\\ \{\dot{q}_e(t)\}\end{Bmatrix} + \left(\begin{bmatrix}[0] & [0]\\ [0] & [\omega_{ee}^2]\end{bmatrix} + \begin{bmatrix}[N_{rr}] & [N_{re}]\\ [N_{er}] & [N_{ee}]\end{bmatrix}\right) \times \begin{Bmatrix}\{q_r(t)\}\\ \{q_e(t)\}\end{Bmatrix} = \begin{bmatrix}[\phi_r]_f^T\\ [\phi_e]_f^T\end{bmatrix}\{f(t)\} \tag{B15}$$

Acknowledgment

This work was supported by the U.S. Air Force Materiel Command, Space and Missile Systems Center, under Contract F04701-93-C-0094.

References

[1]Fleming, E. R., "Launch Vehicle Loads," *Flight-Vehicle Materials, Structures, and Dynamics—Assessment and Future Directions. Vol.1—New and Projected Aeronautical and Space Systems, Design Concepts, and Loads*, Sec. 2, A95-24426, American Society of Mechanical Engineers, New York, 1994, pp. 530–541.

[2]Tinker, M. L., "Liftoff and Landing Design Loads for the Space Shuttle/MIR-3 Mission," AIAA Paper 96-1238, April 1996.

[3]Macheske, V. M., Womack, J. M., and Binkley, J. F., "A Statistical Technique for Combining Launch Vehicle Loads During Atmospheric Flight," AIAA Paper 93-0755, Jan. 1993.

[4]Benfield, W. A., and Hruda, R. F., "Vibration Analysis of Structures by Component Mode Substitution," *AIAA Journal*, Vol. 9, No. 7, 1971, pp. 1255–1261.

[5]Baertlein, J. A., Cwach, E. E., Huleatt, D. R., Shum, S. T., and Stroman, M. M., "Inclusion of Out-of-Plane Aero Data and SRMU Nozzle Hinge Moments in Maximum Airloads Analysis," Space Launch Systems, Loads and Dynamics Dept., Lockheed Martin Corp., MCR-95-2615, NUSTO 95-084, Denver, CO, Nov. 1995.

[6]Christophe, B., and Piet-Lahanier, N., "Flexible Launcher Dynamics Prevision," 45th Congress of the International Astronautical Federation, IAF-94-182, Jerusalem, Israel, Oct. 1994.

[7]Stroman, M. M., and Cwach, E. E., "Flexible Body 6-DOF Loads Trajectory Simulation," Space Launch Systems, Loads and Dynamics Dept., Lockheed Martin Corp., MCR-95-2555, CDRL 231A2-9, Denver, CO, June 1995.

[8]Craig, R. R., *Structural Dynamics: An Introduction to Computer Methods*, 1st ed., Wiley, New York, 1981, pp. 368–371.

[9]Lollock, J. A., "An Improved Acceleration Based Loads Recovery Approach," Vehicle Systems Division, Structural Dynamics Dept., Aerospace Corp., ATM 95-(5530-50)-5, El Segundo, CA, March 1995.

R. Malla
Associate Editor